SPACE WEATHER, VOL. 1, NO. 3, 1013, doi:10.1029/2003SW000007, 2003

A radiation belt-ring current forecasting model

Yihua Zheng
Universities Space Research Association, NASA Goddard Space Flight Center, Greenbelt, Maryland, USA

Mei-Ching Fok
Interplanetary Physics Branch, NASA Goddard Space Flight Center, Greenbelt, Maryland, USA

George V. Khazanov
National Space Science and Technology Center, NASA Marshall Space Flight Center, Huntsville, Alabama, USA

Received 15 April 2003; revised 2 July 2003; accepted 3 October 2003; published 10 December 2003.

[1] A radiation belt-ring current (RB-RC) forecasting model is presented. This model solves the convection-diffusion equation of plasma distribution in the 10 keV to a few MeV range. There are four major auxiliary components to the RB-RC model: a global magnetic field model, an electric field model, a plasma sheet model (plasma source), and a radial diffusion model. All four components are driven by solar wind and interplanetary magnetic field conditions. In this paper, a brief description of the model and input parameters is given. This model has been used to simulate several geomagnetic storms. In particular, the effects of the inductive electric field on the evolution of the radiation belt electron fluxes are investigated in detail via a case study of the 12 August 2000 storm. It is found that, in general, the inductive electric field arising from the time-varying magnetic field can enhance the flux level around geosynchronous orbit during the recovery phase of the storms. The model is validated through comparing the simulation results with the Los Alamos National Laboratory satellite measurements. Further refinement and improvement of the model is also discussed. *INDEX TERMS:* 2753 Magnetospheric Physics: Numerical modeling; 2722 Magnetospheric Physics: Forecasting; 2720 Magnetospheric Physics: Energetic particles, trapped; 2730 Magnetospheric Physics: Magnetosphere—inner; *KEYWORDS:* radiation belt-ring current (RB-RC) forecasting model, inductive electric field, kinetic convection-diffusion equation, driven by solar wind and IMF conditions

Citation: Zheng, Y., M.-C. Fok, and G. V. Khazanov, A radiation belt-ring current forecasting model, *Space Weather*, *1*(3), 1013, doi:10.1029/2003SW000007, 2003.

1. Introduction

[2] Radiation belt and ring current plasmas are hazardous to spacecraft systems and to humans in space. It is very important to predict and forecast the developments of these energetic plasmas and provide warnings early enough for appropriate actions to be taken. This motivates the development of a radiation belt and ring current forecasting model, which is capable of predicting the energetic plasma intensities in the inner magnetosphere ($2-12\ R_E$), over an energy range of 10 keV to a few MeV.

[3] The transport of plasmas in the magnetosphere is controlled by the magnetic and electric fields in which the particles are embedded. *Fok et al.* [1999] simulated substorm injections with various structures of the convection electric field and magnetic fields. They found that both magnetic dipolarization (inductive electric field) and strong convection are required to transport plasmas in the magnetotail earthward to inside the geosynchronous orbit. Using test particle code under the electromagnetic field output from MHD simulation, *Hudson et al.* [1996] simulated particle energization in the interplanetary shock at the dayside magnetopause. They found new electron and proton belts were formed at dipole L shell $\sim$2.5. These studies clearly showed that the electric and magnetic structures and their variations with time are crucial in transport and energization of radiation belt and ring current particles. Other important factors influencing energetic plasma distributions in the inner magnetosphere are the densities and temperatures of the plasma sheet, which is the major source of radiation belt and ring current particles. *Kozyra et al.* [1998] simulated the growth and recovery of the 2–6 November 1993 magnetic storm with their ring current model driven by the dynamic fluxes at the geosynchronous orbit. During this storm interval, a high-density plasma sheet was observed. They found that the super dense plasma sheet had a remarkable impact on the ring current intensity and a factor of 3 change in the plasma sheet density produced a similar factor of enhancement in the strength of the ring current. This study illustrates the importance of near-Earth plasma sheet prediction in the success of radiation belt and ring current forecasting.

[4] Radiation Belt has been an area of active research since its discovery in the early space era [*Van Allen*, 1959]. Existing models of the radiation belt include the NASA AE8 (for electrons) and AP8 (for protons) model [*Sawyer and Vette*, 1976; *Vette*, 1991], Li's radial diffusion model [*Li et al.*, 2001], the radiation belt model developed at Air Force [*Albert et al.*, 2001], and the Salammbô code [*Beutier and*

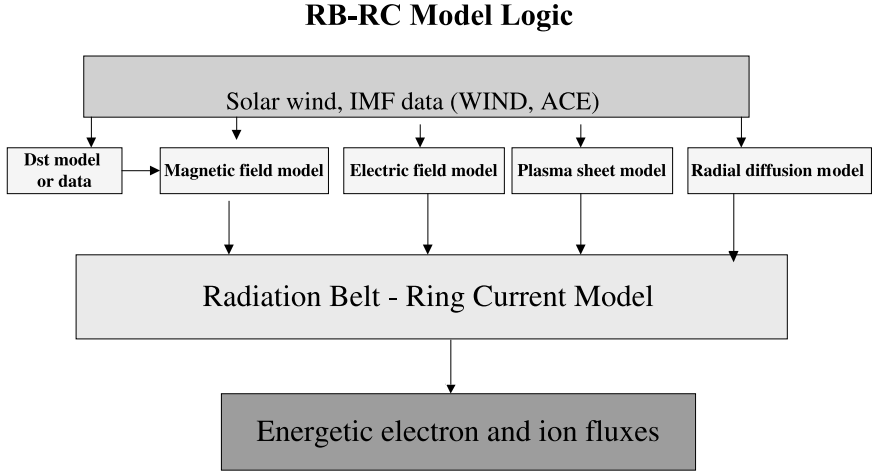

Figure 1. The radiation belt-ring current (RB-RC) model logic and its components.

Boscher, 1995; *Beutier et al.*, 1995; *Bourdarie et al.*, 1997]. The NASA model is an empirical model based on the data collected from more than 20 satellites from the early 1960s to mid-1970s. The limitations of the NASA model are (1) it only gives fluxes in terms of magnetic shell L and energy E in two conditions, solar maximum and solar minimum, and (2) it is a static model based on the data taken in a specific time period, while the trapped radiation belt environment is much more complex and dynamic and has solar cycle, seasonal, and geomagnetic activity dependence. Both Li's model and the model developed at Air Force are based on the radial diffusion equation. Li's model can give remarkably good daily averaged electron flux prediction at geosynchronous orbit using only solar wind and interplanetary magnetic field (IMF) input, and the Air Force model gives a fairly good result of particle fluxes in a wide energy range as well. However, both models are limited to one dimension and require the fitting or tweaking of the diffusion coefficients [*Li et al.*, 2001; *Albert et al.*, 2001]. Salammbo code is the first global model in the sense that the earlier version [*Beutier and Boscher*, 1995; *Beutier et al.*, 1995] of the code provides fluxes in three-dimensional (3-D) phase space (energy, equatorial pitch angle, magnetic shell parameter L), and the later version [*Bourdarie et al.*, 1997] gives fluxes in 4-D phase space with an addition of local time dependence. The model presented in this paper is similar to the 4-D Salammbo model in that it solves the kinetic convection-diffusion equation. But unlike the Salammbo code, in which the dipole magnetic field is employed, our model uses a realistic time-varying magnetic field (T96 model) and electric field model (Weimer 2000 model) so that the inductive effects due to changing magnetic and electric field are included.

[5] The core of our forecasting model is based on the kinetic models of the inner magnetosphere developed by Fok, Moore, Khazanov, and coworkers [*Fok and Moore*, 1997; *Fok et al.*, 1996, 2001; *Khazanov et al.*, 1998, 1999]. This model solves the kinetic convection-diffusion equation of plasma distribution functions in the vicinity of L = 2 to 12 and in the energy range of 10 keV-1 MeV for ions and 10 keV-5 MeV for electrons. Particle drifts as a result of magnetic field gradient and curvature, and the electric fields associated with the Earth's rotation, convection field, as well as the inductive field due to time-varying magnetic field, are considered. The model also takes into account losses along particle drift paths. These models have been used extensively to simulate evolution of energetic plasmas during magnetic storms and substorms [*Khazanov et al.*, 1998; *Fok and Moore*, 1997; *Fok et al.*, 1995, 1996, 1999, 2001]. Generally, very good agreements with observations have been obtained.

[6] In this paper, we will present the radiation belt-ring current model and its simulation results. In section 2 the forecasting scheme is presented. In section 3 we briefly describe the model and its input parameters. In section 4 the model is validated by comparing the simulation results with the Los Alamos National Laboratory (LANL) satellite observations during a magnetic storm on 12 August 2000. Summary and future work are given in section 5.

2. Forecasting Scheme

[7] Our forecasting scheme is based on the solar wind and IMF conditions and their prediction. The coupling processes of the solar wind with the Earth magnetosphere create a very complicated space plasma environment in this region. It is believed that the solar wind drives a geomagnetic field configuration in the outer magnetosphere, creates the magnetospheric electric field, stimulates plasma sheet plasma injection, and controls plasma transport through radial diffusion coefficients. These are the four main components needed to be considered in order to simulate the Radiation Belt (RB) and Ring Current (RC) environment. Figure 1 shows the logic diagram of our RB-RC prediction model. All the input models are parameterized with solar wind (SW) parameters. The top rectangle of Figure 1 contains the observed SW plasma and interplanetary magnetic field parameters that drive the five boxes below: the *Dst* index, the geomagnetic field,

the convection electric field, particle injection from the plasma sheet, and the radial diffusion coefficient model. It should be mentioned that this model is purely solar wind and IMF-driven and the main components are the geomagnetic field, the convection electric field, the particle source of the plasma sheet and the radial diffusion coefficient model. *Dst* index is needed because the geomagnetic field model used here is the T96 model that takes *Dst* as one of its input parameters (the latest version T01 uses the time history of solar wind and IMF conditions instead, such as G1 and G2 parameters [*Tsyganenko*, 2000a, 2000b]). Once these four models are set up, we start RB and RC simulation and generate electron and ion fluxes in the magnetosphere.

[8] Numerous theoretical and empirical models have been developed to simulate the *Dst* index, the global magnetic and electric configurations, and the plasma sheet distributions as a function of solar and geomagnetic conditions [*Klimas et al.*, 1997, 1998; *Tsyganenko*, 1995; *Hilmer and Voigt*, 1995; *Slinker et al.*, 1998; *Volland*, 1978; *Weimer*, 1995, 2001; *Borovsky et al.*, 1998; *Ebihara and Ejiri*, 2000]. Most of these models are driven by the solar wind conditions at the magnetopause or by geomagnetic indices measured on the ground. Many of these data are available in near real time in public domains. Following the logic shown in Figure 1, our RB-RC model is driven only by the solar wind and IMF conditions. This model is also designed to have the feasibility to adopt various magnetic field, electric field, plasma sheet, and radial diffusion models.

3. Models and Input Parameters

[9] The details of the RB-RC model can be found in the work of *Fok and Moore* [1997] and *Fok et al.* [2001], so only a brief description is given here. The temporal variation of the phase space density of a particle species, *s*, is calculated by solving the following bounce-averaged Boltzmann transport equation

$$\frac{\partial \bar{f}_s}{\partial t} + \langle \lambda_i \rangle \frac{\partial \bar{f}_s}{\partial \lambda_i} + \langle \phi_i \rangle \frac{\partial \bar{f}_s}{\partial \phi_i} = \frac{1}{\sin 2\lambda_i} \frac{\partial}{\partial \lambda_i} \left(\sin 2\lambda_i D_{\lambda_i \lambda_i} \frac{\partial \bar{f}_s}{\partial \lambda_i} \right) - \frac{\bar{f}_s}{\tau_l} - \left(\frac{\bar{f}_s}{0.5\,\tau_b} \right)_{\text{loss cone}}, \quad (1)$$

where $\bar{f}_s = \bar{f}_s(t, \lambda_i, \phi_i, M, K)$, is the average distribution function on the field line between mirror points. λ_i and φ_i are the magnetic latitude and local time, respectively, at the ionosphere foot point of the geomagnetic field line. M is the relativistic magnetic moment, and $K = JI\sqrt{8m_oM}$, where J is the second adiabatic invariant. The motion of the particles is described by their drifts across field lines which are labeled by their ionospheric foot points. The shape of a field line changes but the ionospheric foot points are treated to be fixed [*Birmingham and Jones*, 1968] and essentially dipolar.

[10] The left hand side of equation (1) represents the drifts of the particle population and the terms on the right hand side of equation (1) refer to diffusion and losses. The calculation of the bounce-averaged drift velocities, $\langle \lambda_i \rangle$ and $\langle \phi_i \rangle$, were described in detail in the paper of *Fok and Moore* [1997]. The term $\langle \lambda_i \rangle$ represents the radial transport and $\langle \phi_i \rangle$ is the azimuthal drift velocity. These drifts include gradient and curvature drift, and $\mathbf{E} \times \mathbf{B}$ drift from convection and corotation electric fields. The effects of inductive electric field due to time-varying magnetic field is also taken into account implicitly in the model. We have assumed that field lines are rooted at the ionosphere, so the inductive electric field there is zero. However, the shapes of field lines at higher altitudes vary as a function of time according to the magnetic field model. If field lines are prefect conductors, the field line motion at high altitudes, e.g., at the equator, will generate an induction electric field with the form

$$\mathbf{E}_{ind} = -\mathbf{v}_o \times \mathbf{B}_o, \quad (2)$$

where v_o and B_o are the field line velocity and magnetic field at the equator. The $\mathbf{E} \times \mathbf{B}$ drift associated with this induction electric field would be

$$\mathbf{v} = \frac{\mathbf{E}_{ind} \times \mathbf{B}_o}{B_o^2} = \mathbf{v}_o, \quad (3)$$

Equation (3) illustrates the "frozen in field line" character as particles move with field lines during the field line motion. Thus the total $\mathbf{E} \times \mathbf{B}$ drift of a particle in the equatorial plane is

$$\mathbf{v}_{\mathbf{E}\times\mathbf{B}} = \frac{\mathbf{E}_{ind} \times \mathbf{B}_o}{B_o^2} + \frac{-\nabla\Phi \times \mathbf{B}_o}{B_o^2}, \quad (4)$$

where the potential Φ is mapped from along field lines from the ionosphere. The first term is the velocity of the equatorial mapping point of a field line with fixed ionospheric end point. The effect of induction electric field is included through the particle motions associated with field line reconfiguration. In the calculation the gradient-curvature drift and other quantities are varied continuously according to the instantaneous magnetic configuration. At the same time, the mapping of particle distribution from the ionospheric grids to the magnetosphere is adjusted accordingly.

[11] The first term on the right hand side of equation (1) represents particle diffusion in λ_i as a result of electric and magnetic field fluctuations. Diffusion in latitude in the ionosphere is equivalent to radial diffusion in the magnetosphere (i.e., at the equator). The relation between radial diffusion coefficient (D_{LL}) and the corresponding coefficient in latitude $D_{\lambda_i\lambda_i}$ is given as [*Fok et al.*, 2001]

$$D_{\lambda_i\lambda_i} = D_{LL} \frac{\cos^4 \lambda_i}{r_i \sin 2\lambda_i}, \quad (5)$$

where r_i is the ionospheric distance in Earth radius (R_E). The diffusion term is followed by the loss terms. Loss due to charge exchange loss for ions is treated as a decay time, τ_l. Particles in the loss cone, the boundary of which is assumed to correspond to mirror height of 120 km, are assumed to have a lifetime of one-half bounce period ($0.5\,\tau_b$).

[12] Equation (1) represents a combined convection-diffusion approach in solving for the radiation belt distribution. During magnetic storms and substorms, the magnetic and electric fields undergo large-scale variations or reconfigurations. This global topology structure and its dynamic changes determine the overall charged particle convection transport patterns, which is taken care of by the drifts in left-hand side of equation (1). At the same time, **B** and **E** continually fluctuate over a range of oscillation frequencies and amplitudes. With a specific form of the power spectrum adopted, an appropriate radial diffusion coefficients can be formulated either expressed as functions of the L shell parameter, or, equivalently, as functions of the invariant magnetic latitude as indicated in equation (1). By considering both convection and diffusion simultaneously, we can realistically simulate the convection-dominated low-energy particles, the diffusion-dominated high-energy particles, and the particles of the ring current range where both processes are effective. Furthermore, we are able to resolve the transient behaviors of plasmas due to the rapid magnetic-electric reconfiguration from the diffusion effects of relatively longer time-scales.

[13] As shown in Figure 1, in order to run the kinetic model represented by (1), we have to first specify the electric and magnetic fields and the particle distribution on the nightside boundary, which is set at 12 R_E. We have done some research to find the most suitable models. Our preliminary selections are the Tsyganenko 1996 (T96) model [*Tsyganenko*, 1995] for magnetic field and the empirical model of Weimer 2000 [*Weimer*, 2001] for convection electric field. Both the T96 and the Weimer models are parameterized by solar wind and IMF conditions. The T96 model also requires hourly index *Dst* as input. It should be mentioned that for case study, we use the Kyoto provisional *Dst* index. For the forecasting purpose, we use the *Dst* prediction model by *Klimas et al.* [1997, 1998]. For the plasma sheet distribution at nightside boundary (12 R_E), kappa distribution (kappa = 3 for electrons and kappa = 4 for protons) is assumed with density and characteristic energy driven by solar wind density and velocity as follows:

$$Nps(t) = [0.02*Nsw(t - 3\ \mathrm{hr}) + 0.316]*\sqrt{\mathrm{amu}}$$

$$Eo(t) = 0.0128*Vsw(t - 3\ \mathrm{hr}) - 1.92 \quad \text{for electrons} \qquad (6)$$

$$Eo(t) = 0.0120*Vsw(t - 3\ \mathrm{hr}) - 1.80 \quad \text{for ions,}$$

where *Nps* is the plasma sheet density in cm^{-3}, and *Nsw* is the solar wind density in cm^{-3}. *Vsw* is the solar wind speed in kilometers per second, and *Eo* is in units of keV. Notice there is a 3-hour time lag between the solar wind and the nightside boundary. The boundary condition on the dayside is not important and is modeled in a simple manner. The dayside boundary distribution is assumed to be a Maxwellian with constant temperature (0.3 keV) and density (5 cm^{-3}).

[14] For radial diffusion coefficient, we adopt the model of *Li et al.* [2001], in which the diffusion coefficient is driven by solar wind and IMF conditions. Just like the classical diffusion coefficient [*Schulz*, 1991], the radial diffusion coefficient used by *Li et al.* [2001] is L^{10} dependent. The difference lies in the factor D_0, where Li's is parameterized by solar wind and IMF conditions. The underlying assumption is that the radial diffusion caused by the magnetic and electric field fluctuations ultimately comes from the fluctuating quantities of solar wind and IMF.

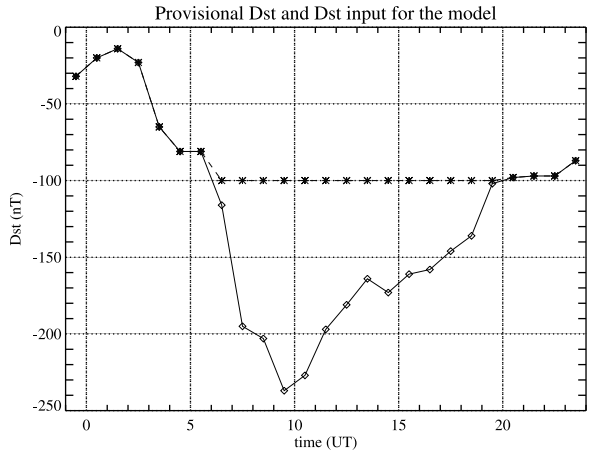

Figure 2. *Dst* index of 12 August 2000 magnetic storm. The provisional data are plotted as diamonds and the input values for T96 are plotted as asterisks.

[15] Initial condition is assumed to be isotropic in local time and in pitch angle. We use the result of NASA AE-8 and Ap-8 models as the initial condition, which in fact is not very important to the subsequent development of the plasma distributions, after a transit of few hours.

[16] Our RB-RC model has been used to simulate the radiation environment during several geomagnetic storms under various geomagnetic conditions. Taking the 12 August 2000 and 1–7 May 1998 events as examples, we will present the calculated electron fluxes from the model and compare them with the geosynchronous particle data from LANL satellites.

4. Simulation Results: Case Studies

[17] Unlike previous simulations reported by [*Fok et al.*, 1996, 1999, 2001; *Fok and Moore*, 1997], where the roles of the inductive electric field associated with substorm dipolarization were studied and the inductive electric field was modeled in a single substorm cycle through a time series of different magnetic field level indicating the magnetic configuration, this investigation studies the effects of inductive electric field purely due to the time-varying nature of the magnetic field. The inductive electric field in this paper comes naturally from the time varying nature of the solar wind and IMF conditions, which drives the global magnetic field configuration via the T96 model.

[18] The RB-RC model is used to simulate the electron fluxes during the storm on 12 August 2000 (See Figure 2 for its *Dst* index). The model outputs electron differential

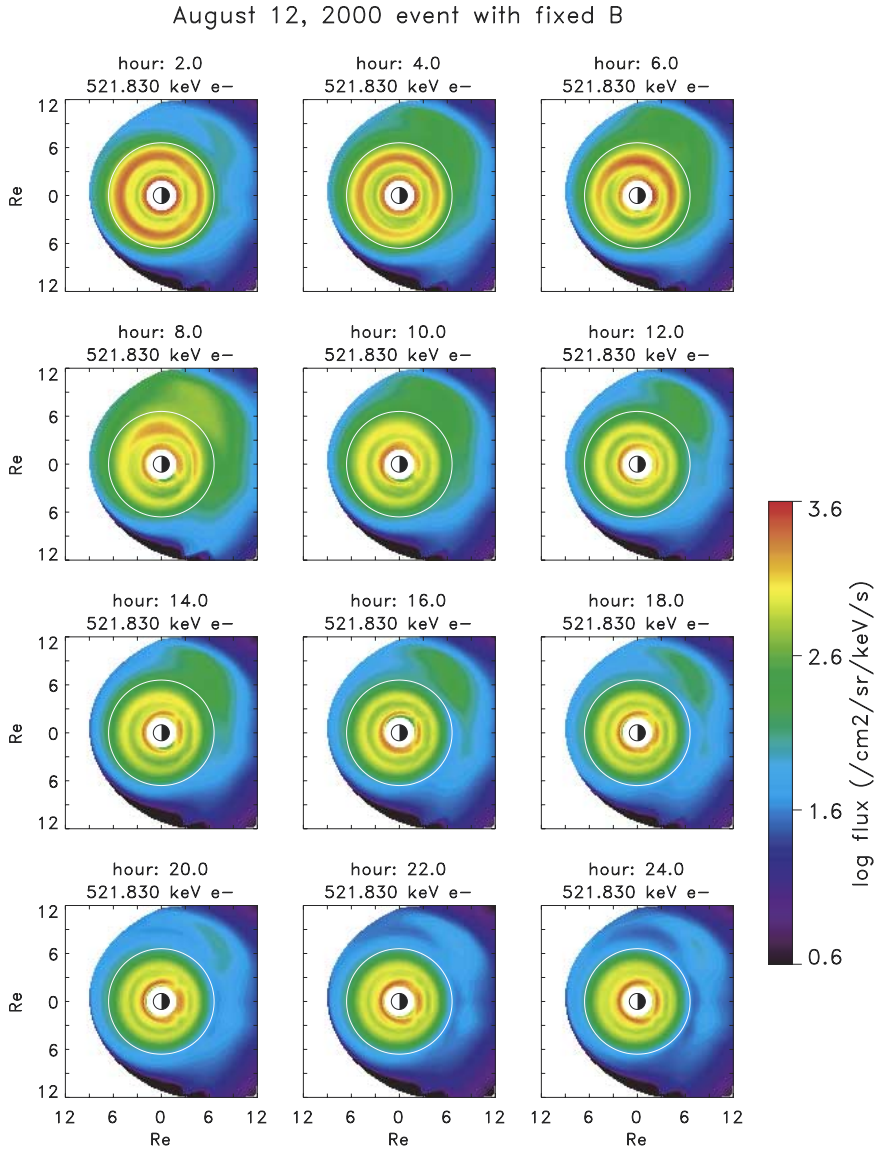

Figure 3. The simulation result of 522 keV electron flux at the equator on 12 August 2000. The magnetic field configuration is from the T96 model, but it is kept constant with time.

fluxes as functions of time, location in 3-D space, energy (10 keV−5 MeV) and pitch angle. In order to see how the inductive electric fields affect radiation belt electron fluxes, we illustrate our results with this 12 August 2000 event. (1) We run our storm simulation under fixed magnetic field configuration by keeping the input parameters (solar wind dynamic pressure (PDYN), *Dst*, IMF *By* and *Bz*) of the T96 model unchanged. (2) We run the simulation under time-varying T96 magnetic field configuration driven by the solar wind and IMF data from the ACE satellite (5-min resolution). The data are propagated from the ACE satellite position to the subsolar point at the dayside magnetopause. The global magnetic field configuration is updated every tf. In this case, tf = 600 seconds (10 min). To ensure smooth transition from one configuration to the next one, the input solar wind and IMF data are averaged with a time window of 4.4 tf. For instance, the value of *By* used in t to t + tf is the average of the *By* data from time t − 1.7 tf to t + 2.7 tf. For the *Dst* in t to t + tf, we use the linear interpolated value at time t. We restrain the magnetic field change to be slow and smooth to separate the effects due to fluctuations in short timescales, which are modeled by the radial diffusion in equation (1). It should be noted here that the input parameters for the T96 model all have their range limits ($-100 \leq Dst \leq 20$, 0.5 nPa $\leq$ PDYN $\leq$ 10 nPa, -10 nT $\leq$ By $\leq$ +10 nT, -10 nT $\leq$ Bz $\leq$ +10 nT). These are the limits given in the T96 document. The limits are applied in the RB-RC model except the lower limit of the solar wind dynamic pressure. We use 1.2 nPa $\leq$ PDYN $\leq$ 10 nPa instead in order to make the subsolar point less than 12 Re (our model boundary). The input data outside the range are set to the corresponding end values. For

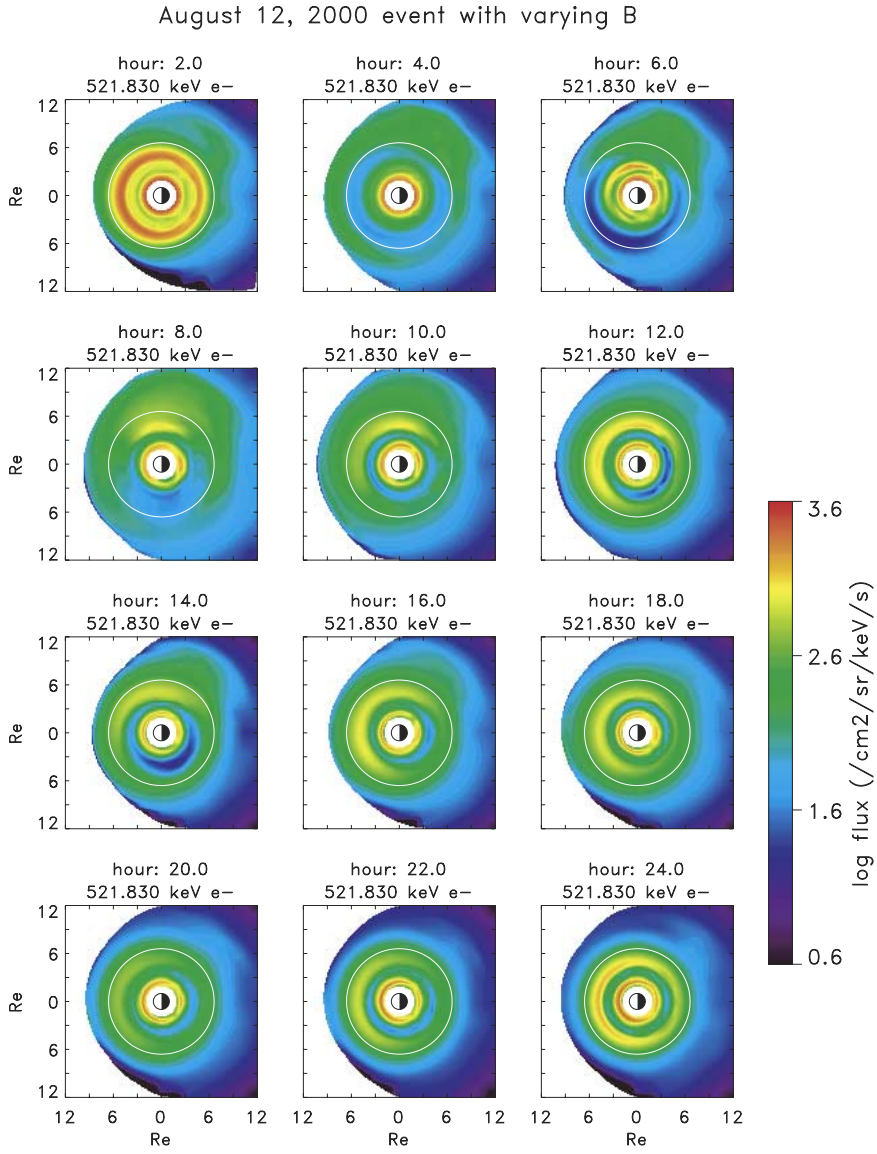

Figure 4. Same as Figure 3 except that the magnetic field configuration from the T96 model is varying with time.

example, the *Dst* value smaller than −100 nT is set as −100 nT and the *Dst* value larger than 20 nT is set as 20 nT (see Figure 2 for the result of this).

[19] Figure 3 shows the evolution of 522 keV electron pitch angle-averaged fluxes at the equatorial plane under fixed magnetic field. In comparison, Figure 4 shows the same energy electron fluxes under the time varying magnetic field configuration. From Figures 3 and 4 we can see that with fixed **B**, the 522 keV electron fluxes reside mostly inside the geosynchronous orbit (the white circle in the plots). While in the case of varying **B** (the existence of inductive electric field), we can see that as the storm progresses, the electron fluxes have obvious two belt structure: one is inside 3 R_E, and the other one is centered at ~4.5 R_E. There is enhancement of fluxes near the geosynchronous orbit comparing to the case of fixed **B**. The overall fluctuations in time in the electron fluxes in the varying **B** case are due to the adiabatic energization or deceleration of particles.

[20] To test how well our model could reproduce the observed radiation belt particle fluxes, we compared the simulated electron fluxes of the two cases at the geosynchronous orbit with the LANL data obtained from Synchronous Orbit Particle Analyzer (SOPA) measurements. Figure 5 shows the comparisons under the two conditions. Figure 5 (left) shows the results for the fixed **B** case and the middle panels are those for the case of varying **B**. These two panels show the time series of simulated fluxes at the same locations as the LANL satellites. The LANL satellite data are shown in Figure 5 (right).

[21] We can see that for both cases, the overall fluxes from the model results are a little bit higher than the observed fluxes, yet the simulation results captures the general fea-

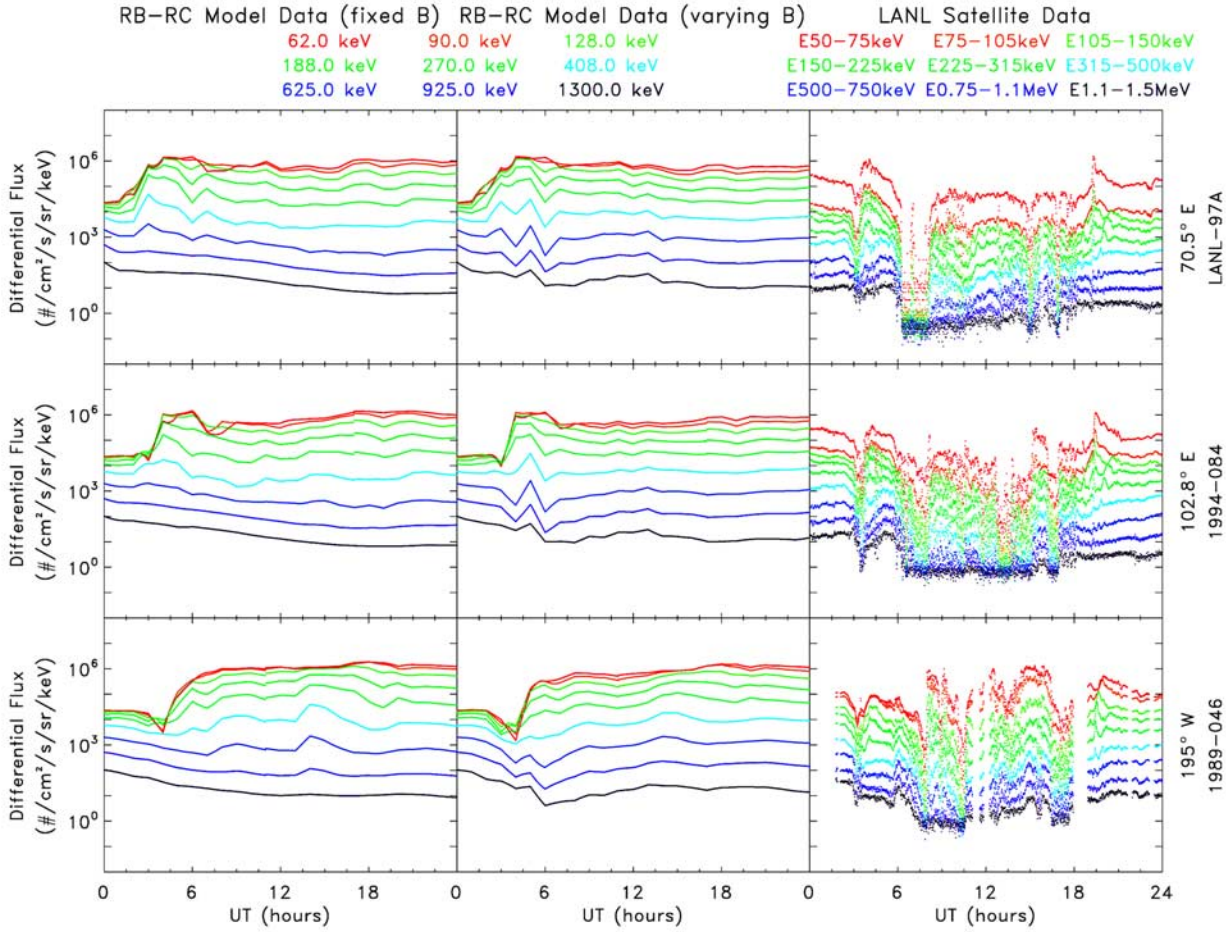

Figure 5. Comparison between the calculated differential fluxes and those of Los Alamos National Laboratory (LANL) satellite observations on 12 August 2000. (left) Results for the fixed magnetic field configuration. (middle) Time-varying magnetic field configuration. (right) Measurements from the LANL satellites.

tures reasonably well. We believe the matching of magnitude can be achieved by choosing a better model of plasma sheet source at the 12 R_E boundary. For the case of fixed **B** in Figure 4, the fluxes of the electrons whose energy are above 500 keV decrease steadily as time evolves, while in the LANL data, we see a gradual increase of fluxes at those energies in the recovery phase of the storm (later part of the day). In contrast, for the case of varying B (Figure 5, middle) the higher energy fluxes increase during the recovery phase and have much better agreement with the data than those with fixed **B**. We can see that the inductive electric field has larger effects on higher-energy particles. The inductive electric field can change the particle drift paths from the open to the closed, and thus more plasmas are trapped. With the varying magnetic field, the model captures the sharp decrease seen in the LANL geosynchronous fluxes around 0600 UT during the storm main phase.

[22] It should be mentioned that in order to see whether how the global magnetic field is varied has any effect on the radiation belt fluxes, we did the same 12 August 2000 storm simulation under two other varying magnetic field configurations. In the results shown above the solar wind and IMF data are smoothed in a time window of 44 min and the global magnetic field from T96 model is updated every 10 min. The other two configurations of magnetic field are (1) The solar wind and IMF are smoothed in 88-min interval, and the global magnetic field is updated every 20 min. (2) The solar wind and IMF are in 22-min interval, and the magnetic field is updated every 5 min. Our results show that the radiation belt electron fluxes are about the same for all the three varying magnetic field configurations. This indicates that the fluxes of the radiation belt electrons are insensitive to how we vary the magnetic field configurations in the small range as long as the input solar wind IMF data have been smoothed and are steady relative to the timescale of particle drift periods. The effects of the inductive electric field can be seen from the simulation results done on other geomagnetic storms (25 September 1998 and 1−7 May 1998) as well. Generally speaking, the inductive electric field due to the varying global magnetic field increases the fluxes level

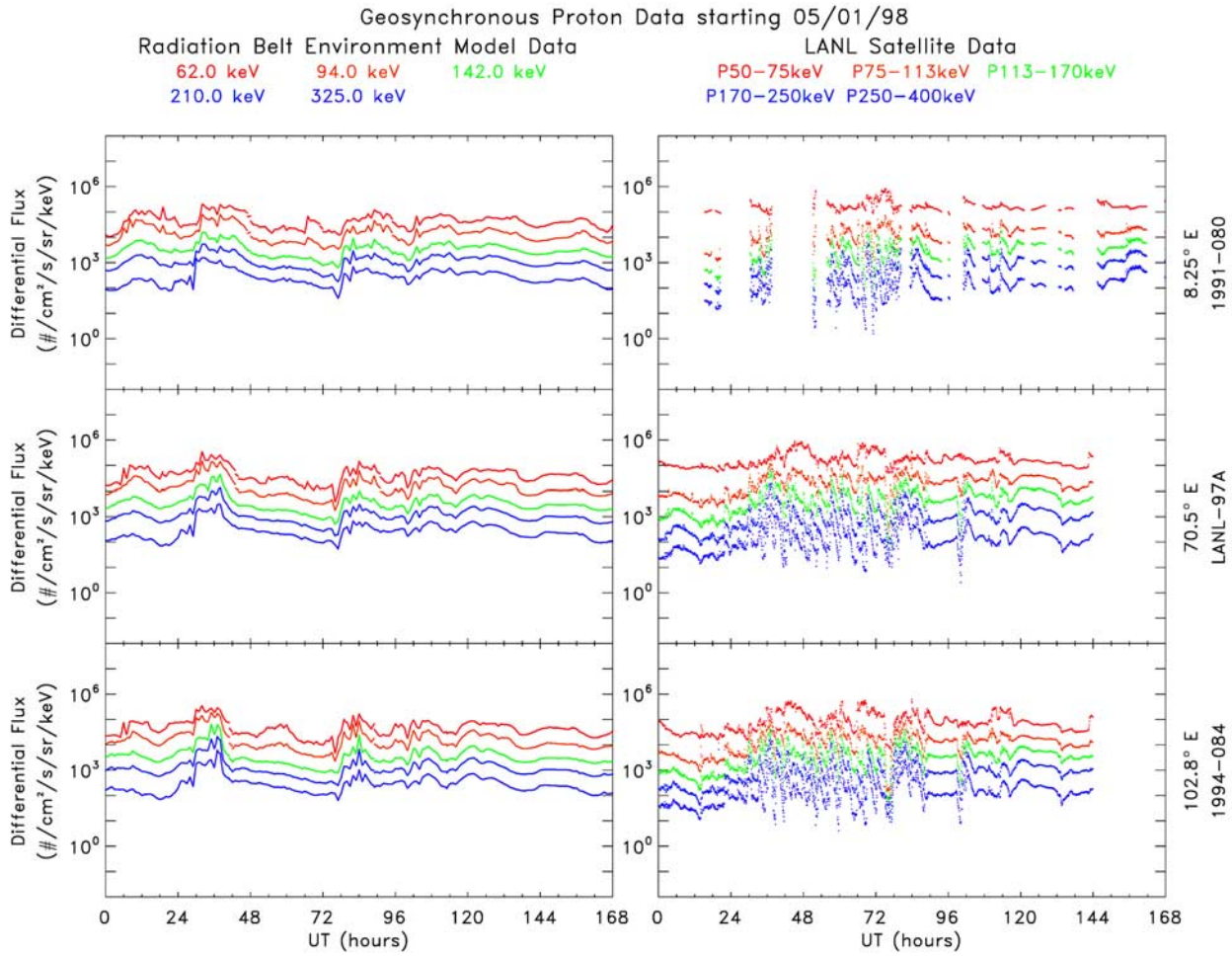

Figure 6. Comparison between the calculated differential fluxes and those of LANL satellite observations on 1–7 May 1998. (left) Results from the RB-RC model. (right) Measurements from the LANL satellites.

around geosynchronous orbit during the recovery phase of the storms.

[23] For the purpose of further validating the RB-RC model, the simulated proton fluxes of 1–7 May 1998 storm and the corresponding LANL satellite measurements are shown in Figure 6. The main phase of this storm is long and contains two minimum *Dst* values, with the first one of −85 nT at 1800 UT on 2 May and the second one of −205 nT at 0600 UT on 4 May. We can see from Figure 6 that the simulation results agree with the measurements fairly well. However, the substorm-associated features seen in the LANL data in 2–4 May are not reproduced in the model. One should note that this model is not designed to forecast substorm signatures, which are very difficult to

Table 1. RMS Error σ Between the Model and the LANL Data of 12 August 2000[a]

Energy, kev	Fixed B With LANL-97A	Varying B With LANL-97A	Fixed B With 1994-084	Varying B With 1994-084	Fixed B With 1989-046	Varying B With 1989-046
62.0	1.55	1.54	1.53	1.47	1.13	1.05
90.0	2.25	2.17	2.15	2.04	1.46	1.30
128.0	2.30	2.23	2.35	2.22	1.90	1.69
188.0	2.24	2.23	2.35	2.27	2.04	1.81
270.0	2.15	2.27	2.23	2.29	2.08	1.87
408.0	1.77	2.01	1.88	2.07	1.84	1.74
625.0	1.48	1.77	1.50	1.69	1.34	1.40
925.0	1.04	1.29	1.03	1.17	0.96	1.10
1300.0	0.63	0.71	0.60	0.66	0.55	0.64

[a]LANL, Los Alamos National Laboratory.

Table 2. RMS Error σ Between the Model and the LANL Data of 1–7 May 1998 Event

Energy, keV	Model With 1991-080	Model With LANL-97A	Model With 1994-084
62.0	0.67	0.70	0.54
94.0	0.47	0.48	0.53
142.0	0.45	0.44	0.48
210.0	0.50	0.45	0.49
325.0	0.61	0.55	0.54

predict anyway. The prediction of substorm occurrence or timing is still far from mature.

[24] The quantitative measure of the model efficiency is calculated from the RMS between the logrithmic value of the model fluxes and the LANL measured fluxes (σ) and shown in Tables 1 and 2 for the cases plotted in Figures 5 and 6, respectively.

[25] From Table 1 we can see that the model calculation is generally 1–2 orders off the measurements of LANL satellites for the event of 12 August 2000. However, with a smaller energy range (low-energy particles only) and therefore a finer energy grid the model result is improved significantly, ~0.5 order magnitude off the LANL data for the event of 1–7 May 1998. This reinforces the point that we are about to make in section 5: a bi-kappa distribution function to model plasmas of two populations (hot and cold) is needed at the nightside boundary of the model. Adjusting the parameters of a single kappa distribution only can improve the fluxes at one end, either at the lower energy end or higher energy end, but not both. Of course, a better magnetic field model (T01) can be of help for the improvement of the RB-RC model result.

5. Summary and Future Work

[26] The purpose of this paper is to introduce our radiation belt-ring current (RB-RC) forecasting model and to investigate the roles of the inductive electric field on the evolution of energetic plasmas. The role of the inductive electric field associated with substorms and the global convection electric field associated with storms to the ring current/radiation belt development has been a constant debate in the space science community. Although much simulation work has been done on the inductive electric field and its importance of transporting and energizing the magnetospheric plasmas [*Fok et al.*, 1996, 1999, 2001; *Li et al.*, 1993, 1999], the role of inductive electric field is usually studied in an externally imposed fashion. The work presented here explores the inductive electric field naturally accompanying a varying magnetic field configuration. The simulation results show that with the inductive electric field from the varying **B**, our RB-RC model produces comparable electron fluxes as the observations. During the recovery phase of a storm, the inductive electric field energizes and causes trapping of plasmas, and is able to enhance the electron fluxes near the geosynchronous orbit.

[27] We have incorporated pitch angle diffusion due to plasmaspheric hiss to our model. The simulation result has shown that it has little effect on electron flux variations during magnetic storms. In the future we will implement energy diffusions due to interactions with whistler mode chorus to the model. To further improve our model, we will develop a better model of the plasma sheet particle distribution at the model nightside boundary. As we know, the boundary condition is critical to the solution of any partial differential equation and naturally it applies to our RB- RC model described here. We will explore the bi-kappa distribution of plasma sheet plasmas at the model boundary (one represents the cold population and the other represents the hot population) [*Wang et al.*, 2001].

[28] Our RB-RC model is capable of radiation belt/ring current environment now-casting given the solar wind input from ACE/WIND satellites. Our another future goal is to couple our model with a solar wind forecasting model [*Akasofu*, 2001] so that the model will be able to do the radiation belt/ring current forecasting a few days ahead of time.

[29] **Acknowledgments.** We are grateful for the useful discussions with Richard Wolf. We thank Peggy Sloan for developing the visualization software. The LANL SOPA data are provided by Geoff Reeves. This work is supported by the University Partnering for Operational Support (UPOS) Program.

References

Akasofu, S.-I., Predicting geomagnetic storms as a space weather project, in *Space Weather*, *Geophys. Monogr. Ser.*, vol. 125, edited by P. Song, H. J. Singer, and G. L. Siscoe, pp. 329–337, AGU, Washington, D. C., 2001.

Albert, J. M., D. H. Brautigam, R. V. Hilmer, and G. P. Ginet, Dynamic radiation belt modeling at the Air Force Research Laboratory, in *Space Weather*, *Geophys. Monogr. Ser.*, vol. *125*, edited by P. Song, H. J. Singer, and G. L. Siscoe, pp. 281–287, AGU, Washington D. C., 2001.

Beutier, T., and D. Boscher, A three-dimensional analysis of the electron radiation belt by the Salammbô code, *J. Geophys. Res.*, *100*, 14,853–14,861, 1995.

Beutier, T., D. Boscher, and M. France, SALAMMBO: A three-dimensional simulation of the proton radiation belt, *J. Geophys. Res.*, *100*, 17,181–17,188, 1995.

Birmingham, T. J., and F. C. Jones, Identification of moving magnetic field lines, *J. Geophys. Res.*, *73*, 5505–5510, 1968.

Borovsky, J. E., M. F. Thomsen, and R. C. Elphic, The driving of the plasma sheet by the solar wind, *J. Geophys. Res.*, *103*, 17,617–17,639, 1998.

Bourdarie, S., D. Boscher, T. Beutier, J.-A. Sauvaud, and M. Blanc, Electron and proton radiation belt dynamic simulations during storm periods: A new asymmetric convection-diffusion model, *J. Geophys. Res.*, *102*, 17,541–17,552, 1997.

Ebihara, Y., and M. Ejiri, Simulation study on fundamental properties of the storm-time ring current, *J. Geophys. Res.*, *105*, 15,843–15,859, 2000.

Fok, M.-C., and T. E. Moore, Ring current modeling in a realistic magnetic field configuration, *Geophys. Res. Lett.*, *24*, 1775–1778, 1997.

Fok, M.-C., T. E. Moore, J. U. Kozyra, G. C. Ho, and D. C. Hamilton, Three-dimensional ring current decay model, *J. Geophys. Res.*, *100*, 9619–9632, 1995.

Fok, M.-C., T. E. Moore, and M. E. Greenspan, Ring current development during storm main phase, *J. Geophys. Res.*, *101*, 15,311–15,322, 1996.

Fok, M.-C., T. E. Moore, and D. C. Delcourt, Modeling of inner plasma sheet and ring current during substorms, *J. Geophys. Res.*, *104*, 14,557–14,569, 1999.

Fok, M.-C., T. E. Moore, and W. N. Spjeldvik, Rapid enhancement of radiation belt electron fluxes due to substorm dipolarization of the geomagnetic field, *J. Geophys. Res.*, *106*, 3873–3881, 2001.

Hilmer, R. V., and G.-H. Voigt, A magnetospheric magnetic field model with flexible current systems driven by independent physical parameters, *J. Geophys. Res.*, *100*, 5613–5626, 1995.

Hudson, M. K., S. R. Elkington, J. G. Lyon, V. A. Marchenko, I. Roth, M. Temerin, and M. S. Gussenhoven, MHD/particle simulations of radiation belt formation during a storm sudden commencement, in *Radiation Belts*: *Models and Standards*, *Geophys. Monogr. Ser.*, vol. 97, edited by J. F. Lemaire, D. Heynderickx, and D. N. Baker, pp. 57–62, AGU, Washington, D. C., 1996.

Khazanov, G. V., M. W. Liemohn, J. U. Kozyra, and T. E. Moore, Global Superthermal Electron Transport: Photoelectron and Plasma Sheet Electron Sources, *J. Geophys. Res.*, *103*, 23,485–23,501, 1998.

Khazanov, G. V., M. W. Liemohn, E. N. Krivorutsky, J. M. Albert, J. U. Kozyra, and B. E. Gilchrist, Relativistic Electron Beam Propagation in the Earth's Magnetosphere, *J. Geophys. Res.*, *104*, 28,587–28,599, 1999.

Klimas, A. J., D. Vassiliadis, and D. N. Baker, Data-derived analogues of the magnetospheric dynamics, *J. Geophys. Res.*, *102*, 26,993–27,009, 1997.

Klimas, A. J., D. Vassiliadis, and D. N. Baker, *Dst* index prediction using data-derived analogues of the magnetospheric dynamics, *J. Geophys. Res.*, *103*, 20,435–20,448, 1998.

Kozyra, J. U., V. K. Jordanova, J. E. Borovsky, M. F. Thomsen, D. J. Knipp, D. S. Evans, D. J. McComas, and T. E. Cayton, Effects of high-density plasma sheet in ring current development during the November 2–6, 1993, magnetic storm, *J. Geophys. Res.*, *103*, 26,285–26,305, 1998.

Li, X., I. Roth, M. Temerin, J. R. Wygant, M. K. Hudson, and J. B. Blake, Simulation of the prompt energization and transport of radiation particles during March 24, 1991 SSC, *Geophys. Res. Lett.*, *20*, 2423–2426, 1993.

Li, X., D. N. Baker, M. Temerin, G. D. Reeves, and R. D. Belian, Dispersionless injection simulations explore auroral substorm origins, *Eos Trans. AGU*, *80*(36), 413–414, 1999.

Li, X., M. Temerin, D. N. Baker, G. D. Reeves, and D. Larson, Quantitative prediction of radiation belt electrons at geostationary orbit based on solar wind measurements, *Geophys. Res. Lett.*, *28*, 1887–1890, 2001.

Sawyer, D. M., and J. I. Vette, AP-8 trapped proton environment for solar maximum and solar minimum, *NSSDC/WDC-A-R&S 76-06*, Natl. Space Sci. Data Cent., Greenbelt, Md., 1976.

Schulz, M., The magnetosphere, in *Geomagnetism*, vol. 4, edited by J. A. Jacobs, pp. 87–293, Academic, San Diego, Calif., 1991.

Slinker, S. P., J. A. Fedder, and J. Chen, Global MHD simulation of the magnetosphere and ionosphere for 1930–2330 UT on November 3, 1993, *J. Geophys. Res.*, *103*, 26,243–26,250, 1998.

Tsyganenko, N. A., Modeling the Earth's magnetospheric magnetic field confined within a realistic magnetopause, *J. Geophys. Res.*, *100*, 5599–5612, 1995.

Tsyganenko, N. A., A model of the near magnetosphere with a dawn-dusk asymmetry: 1. Mathematical structure, *J. Geophys. Res.*, *107*(A8), 1179, doi:10.1029/2001JA000219, 2000a.

Tsyganenko, N. A., A model of the near magnetosphere with a dawn-dusk asymmetry: 2. Parameterization and fitting to observations, *J. Geophys. Res.*, *107*(A8), 1176, doi:10.1029/2001JA000220, 2000b.

Van Allen, J. A., The geomagnetically trapped corpuscular radiation, *J. Geophys. Res.*, *64*, 1683–1689, 1959.

Vette, J. I., The AE-8 trapped electron model environment, *NSSDC/WDC-A-R&S, 91-24*, Natl. Space Sci. Data Cent., Greenbelt, Md., 1991.

Volland, H., A model of the magnetospheric convection electric field, *J. Geophys. Res.*, *83*, 2695–2699, 1978.

Wang, C.-P., L. R. Lyons, M. W. Chen, and R. A. Wolf, Modeling the quiet time inner plasma sheet protons, *J. Geophys. Res.*, *106*, 6161–6178, 2001.

Weimer, D. R., Models of high-latitude electric potentials derived with a least error fit of spherical harmonic coefficients, *J. Geophys. Res.*, *100*, 19,595–19,607, 1995.

Weimer, D. R., An improved model of ionospheric electric potentials including substorm perturbations and applications to the Geospace Environment Modeling November 24, 1996, event, *J. Geophys. Res.*, *106*, 407–416, 2001.

M.-C. Fok, Interplanetary Physics Branch, NASA Goddard Space Flight Center, Greenbelt, MD 20771, USA.

G. V. Khazanov, National Space Science and Technology Center, NASA Marshall Space Flight Center, Huntsville, AL 35805, USA.

Y. Zheng, Universities Space Research Association, NASA Goddard Space Flight Center, Greenbelt, MD 20771, USA. (yzheng@lepvax.gsfc.nasa.gov)